Published online May 17, 2018

Original Research

Core Ideas

- Dynamics of earthworm activity change macropore networks temporally.
- In the topsoil, macropore numbers were largest in autumn and smallest in summer.
- Temporal dynamics in macropore networks affected their hydrological impact.
- Modeling confirmed that temporal macropore dynamics affect infiltration patterns.

Impact of Temporal Macropore Dynamics on Infiltration: Field Experiments and Model Simulations

Arne Reck,* Conrad Jackisch, Tobias L. Hohenbrink, Boris Schröder, Anne Zangerlé, and Loes van Schaik

Macropores greatly affect water and solute transport in soils. Most macropores are of biogenic origin; however, the resulting seasonal dynamics are often neglected. Our study aimed to examine temporal changes in biopore networks and the resulting infiltration patterns. We performed infiltration experiments with Brilliant Blue on pastureland in the Luxembourgian Attert catchment (spring, summer, and autumn 2015). We developed an image-processing scheme to identify and quantify changes in biopores and infiltration patterns. Subsequently, we used image-derived biopore metrics to parameterize the ecohydrological model echoRD (ecohydrological particle model based on representative domains), which includes explicit macropore flow and interaction with the soil matrix. We used the model simulations to check whether biopore dynamics affect infiltration. The observed infiltration patterns revealed variations in both biopore numbers and biopore–matrix interaction. The field-observed biopore numbers varied over time, mainly in the topsoil, with the largest biopore numbers in spring and the smallest in summer. The number of hydrologically effective biopores in the topsoil seems to determine the number and thereby the fraction of effective biopores in the subsoil. In summer, a strong biopore–matrix interaction was observed. In spring, the dominant process was rapid drainage, whereas in summer and autumn, most of the irrigated water was stored in the examined profiles. The model successfully simulated infiltration patterns for spring, summer, and autumn using temporally different macropore setups. Using a static macropore parameterization the model output deviated from the observed infiltration patterns, which emphasizes the need to consider macropores and their temporal dynamics in soil hydrological modeling.

Abbreviations: CAOS, Catchments as Organised Systems; echoRD, ecohydrological particle model based on representative domains.

Infiltration and distribution of water in the topsoil is a key aspect of soil hydrology and substantially depends on soil structure. Macropores are a fundamental part of soil structure (Beven and Germann, 1982) and often serve as preferential flow pathways. As such, they enhance the infiltration capacity of soils (Ehlers, 1975) and greatly influence water and solute transport through soils (Beven and Germann, 1982, 2013; Jarvis, 2007) and water redistribution in soils (Klaus et al., 2013). Often, macropores are of biogenic origin, meaning their morphology is controlled by the abundance, activity, and lifecycle of the creator (Capowiez et al., 2001, 2014; Botschek et al., 2002; Bastardie et al., 2003, 2005; Felten and Emmerling, 2009). Hence, macropore networks often exhibit a very high spatial, as well as temporal, variability (Daniel et al., 1997; Capowiez et al., 2009; Pelosi et al., 2017).

Biopores are one common representative of macropores and are mainly attributable to soil-dwelling organisms, especially earthworms (Blouin et al., 2013). The hydrological effectiveness of earthworm burrows depends strongly on their network properties, such as pore density (van Schaik et al., 2013), pore connectivity, and pore tortuosity (Allaire-Leung et al., 2000a, 2000b). Furthermore, biopore–matrix interaction influences the effectiveness of biopores for soil water redistribution and drainage (Weiler, 2005). The

A. Reck, T.L. Hohenbrink, and L. van Schaik, Technische Univ. Berlin, Ecohydrology and Landscape Evaluation, Ernst-Reuter-Platz 1, 10587 Berlin, Germany; C. Jackisch, Karlsruhe Institute of Technology, Hydrology, Otto-Amman-Platz 1, 76131 Karlsruhe, Germany; T.L. Hohenbrink and B. Schröder, Technische Univ. Braunschweig, Landscape Ecology and Environmental Systems Analysis, Langer Kamp 19c, 38106 Braunschweig, Germany; B. Schröder, Berlin-Brandenburg Institute of Advanced Biodiversity Research, 14195 Berlin, Germany; A. Zangerlé, Ministère de l'Agriculture, de la Viticulture et de la Protection des consommateurs, Luxembourg. *Corresponding author (a.reck@tu-berlin.de).

Received 4 Aug. 2017.
Accepted 9 Jan. 2018.

Reck, A., C. Jackisch, T.L. Hohenbrink, B. Schröder, A. Zangerlé, and L. van Schaik. 2018. Impact of temporal macropore dynamics on infiltration: Field experiments and model simulations. Vadose Zone J. 17:170147. doi:10.2136/vzj2017.08.0147

biopore–matrix interaction can be reduced in earthworm burrows (Jégou et al., 2001) due to hydrophobic pore–wall linings (Leue et al., 2013, 2015) and increased bulk densities in the drilosphere of earthworm burrows (Rogasik et al., 2014). When soils are extremely dry or cold, earthworms become inactive (Eggleton et al., 2009) and seal their burrows or migrate into deeper layers for diapause (Lavelle, 1988). Then, the maintenance of earthworm burrows is interrupted, and thus the architecture and properties of biopore networks change considerably. Although the overall effect of macropores on infiltration has been studied in field experiments since the early works of Bouma and Dekker (1978), we are not aware of any study dealing with the question of how seasonally varying earthworm activity affects infiltration.

Brilliant Blue is often used as a dye tracer to assess macropore flow. In combination with image analysis, dye tracing proved a powerful tool, allowing for conclusions about the infiltration processes inferred from dye patterns and about the interplay between soil structure and infiltrating water (Zehe and Flühler, 2001; Weiler and Naef, 2003; Weiler and Flühler, 2004; Cey and Rudolph, 2009; van Schaik, 2009; Bogner et al., 2013). One common problem of dye-staining experiments is their unrepeatability and the yield of single "snapshot" information with high spatial but no temporal resolution. Thus, using Brilliant Blue as a stand-alone method for process analysis is challenging, since the temporal dynamics are fully implicit (Jackisch et al., 2017). Recent progress to trace macropore flow on a temporal scale was obtained with time-lapse, noninvasive imaging techniques applied to soil cores (Luo et al., 2008; Koestel and Larsbo, 2014; Sammartino et al., 2015). Allroggen et al. (2015) reached promising results applying noninvasive imaging to measure soil water flow on the plot scale. However, this method still lacks a sufficient resolution for imaging preferential flow and requires further improvement, especially in cases of existing small-scale gradients of the geophysical properties that substantially influence the measurement signal (Koestel et al., 2009). Our suggestion, therefore, is the use of image analysis to receive quantitative data in combination with modeling to extend the snapshot information from dye tracing on a temporal scale and to enable virtual experiments.

Modeling macropore flow remains challenging, notably in terms of transferring its natural characteristics into model concepts (i.e., the presence of nonequilibrium, resulting in the existence of different flow processes and related physical forces). Approaches to solve this issue were reviewed by Šimůnek et al. (2003), Gerke (2006), Köhne et al. (2009), Beven and Germann (2013), and Jarvis et al. (2016). A deficiency of most models is to base water flow solely on Richards' equation wherefore assumptions are required that do not apply for preferential flow (Beven and Germann, 2013). A further deficiency of existing macropore flow models is that they generally neglect the dynamic nature of macropore networks (Jarvis et al., 2016). In our view, testing new model concepts while using observable parameters of temporally dynamic macropore networks might help to achieve a more realistic representation of macropore flow.

Our study aims to examine temporal changes in biopore networks and the resulting infiltration patterns. We therefore analyzed the differences in biopore distributions and infiltration patterns based on experimental field data and model scenarios. We use the term "biopores" when referring to macropores with a distinct biogenic origin; otherwise, the more general term "macropores" is used, which addresses the full spectrum of secondary pores.

Our field data consist of Brilliant Blue profiles from irrigation experiments conducted in spring, summer, and autumn 2015 on five different plots in a pasture field in the Attert catchment, Luxembourg. We used image-derived biopore metrics to parameterize a modeling framework for virtually reproducing the irrigation experiments and obtaining results concerning macropore flow on a temporal scale. We further compared the simulation results of several modeling scenarios with the observed infiltration patterns. Thus, we used the echoRD model ("ecohydrological particle model based on representative domains," Jackisch and Zehe, 2017) to test our assumptions that temporal macropore dynamics need to be considered in soil water flow simulations.

Material and Methods

Study Site

The study was performed on a permanent pasture located in the midwest of Luxembourg near the Attert river catchment outlet (49°46′12″ N, 5°56′54″ E; Fig. 1a). It has been organically farmed for several years. The climate is semi-oceanic (van den Bos et al., 2006) with a mean annual precipitation of 768 ± 127 mm and a mean annual temperature of 10.0 ± 0.6°C (weather station Useldange, reference period 2004–2015).

Soil Description

The geological formations are of Keuper origin (Upper Trias) with sediments comprising variegated marls and clayey sandstones (Colbach, 2003). Within the weathered layer, Luvisols with protovertic or vertic properties (IUSS Working Group WRB, 2015) developed as the dominant soil type. Soil textural classes and bulk densities were determined with 18 samples (Fig. 2) and ranged from silt loam to clay loam with 1.17 ± 0.17 g cm^{-3} in the surface samples and silt loam to clay with 1.51 ± 0.04 g cm^{-3} in the deeper samples.

Laboratory Analysis

For the determination of the hydraulic properties of the soil matrix, we analyzed 11 upper soil (0–20 cm) undisturbed ring samples and seven deeper soil (20–40 cm) undisturbed ring samples using the simplified evaporation method (Schindler, 1980) with HYPROP and WP4C (METER Group) measurement devices. To avoid effective properties, including macropores (Jarvis and Messing, 1995; van Schaik et al., 2010), we fitted the retention curves by setting the maximum of field-measured soil moisture to a saturation of primary pore volume of 90%. The resulting hydraulic conductivity and Mualem–van Genuchten

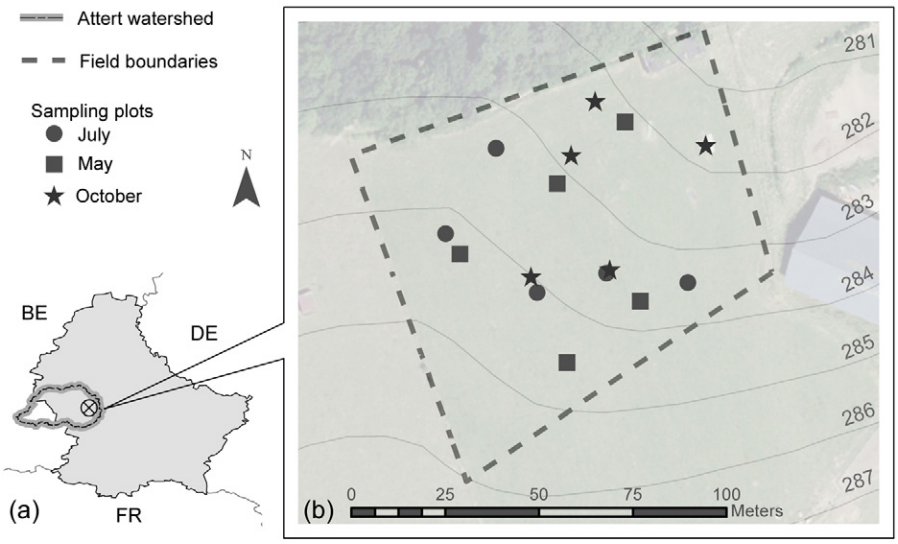

Fig. 1. (a) The location of the study site in Luxembourg (BE, Belgium; DE, Germany; FR, France), and (b) the plots for dye experiments. The distance between contour lines is 1 m, with altitude in meters. The map background is the ArcGIS Luxembourg orthoimagery.

parameters are given in Table 1, along with the respective depth reference.

Infiltration Experiments

In spring (4 May 2015), summer (9 July 2015), and autumn (3 Oct. 2015), dye tracer experiments were performed. During each measurement campaign, five plots (50 × 50 cm^2) were randomly chosen (Fig. 1b). The aim of this sampling design was to obtain representative data covering the spatial heterogeneity of biopores within the field and to allow for investigation of the temporal heterogeneity of biopores. Local heterogeneity and possible catena organization of the soil within the pasture were neglected.

The surface of each selected plot was manually irrigated with 10 L Brilliant Blue solution (4 g L^{-1}) using a watering can. The application was adapted to ensure high infiltration but prevent ponding. We chose this procedure to obtain maximal macropore flow under realistic conditions. Normally, macropore flow occurs as unsaturated flow limited to films along the pore walls, and water supply is usually below the macropore flow capacity (Bouma and Dekker, 1978; Weiler, 2001; Jarvis, 2007; Cey and Rudolph, 2009). Ponding could result in a drastic reduction of the infiltration capacity (Faybishenko, 1995) due to entrapped air (Sněhota et al., 2010), especially in macropores (Luo et al., 2008). Single irrigations lasted ~30 min and, in exceptional cases, up to 60 min, resulting in average rates of 80 mm h^{-1}. Subsequently, the irrigated plots were covered to avoid evapotranspiration. The day after irrigation, each plot was excavated horizontally at the 3-, 10-, and 30-cm depth, resulting in 45 horizontal profiles. In each horizontal profile, biopores were marked by matchsticks and counted, and the profile was photographed from a central position above. Each recorded biopore was assigned to a size class (<2, 2–6, and >6 mm) and a color class (stained or nonstained; note that stained biopores are termed as effective biopores hereafter). Antecedent volumetric soil moisture was measured at five points

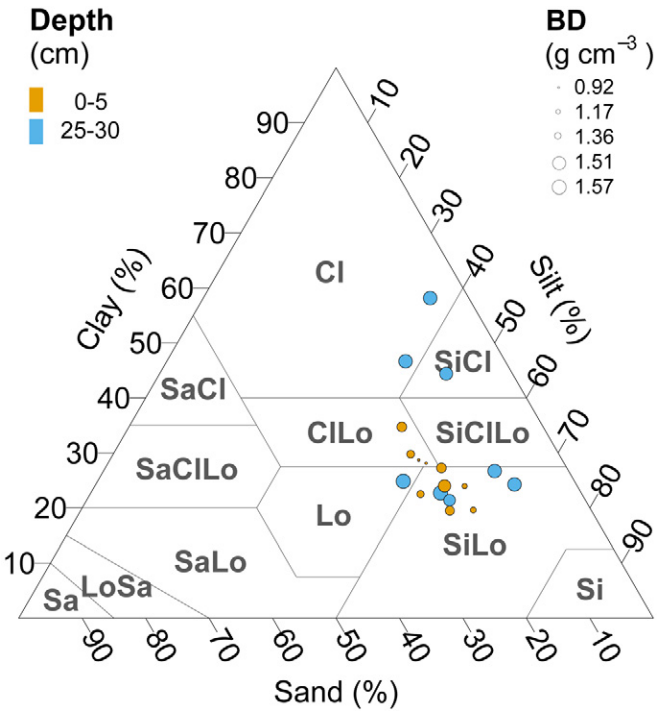

Fig. 2. Texture and bulk density (BD) of soil core samples taken at depths of 0 to 5 and 25 to 30 cm at the study site. Soil textures were measured by sieving and sedimentation analysis (ISO 11277; Deutsches Institut für Normung, 2002). Cl, clay; Lo, loam; Sa, sand; Si, silt.

Table 1. Mualem–van Genuchten parameters used for modeling. The layer boundary between topsoil and subsoil was always positioned at a depth of 20 cm. The soil water retention parameters were obtained by measurements with HYPROP and WP4C on the drying branch. The used soil cores originate from the Wollefsbach subcatchment.

	Parameter†					
Layer	θ_{sat}	θ_{res}	α	n	k_{sat}	Depth
	— cm^3 cm^{-3} —		cm^{-1}		cm d^{-1}	cm
Topsoil	0.50	0.03	0.020	1.27	17.63	0–20
Subsoil	0.47	0.02	0.023	1.25	11.21	20–70

† θ_{sat}, saturated water content; θ_{res}, residual water content; a, inverse air-entry pressure; ksat, saturated hydraulic conductivity. a and n are shape parameters of the water retention function.

in each examined depth using frequency domain reflectometry (FDR) probes (WET sensor, Delta-T devices). During the summer campaign, dry soil conditions inhibited the use of soil moisture probes, so soil moisture content was obtained from the nearby hydrometeorological monitoring station (Zehe et al., 2014).

Compared with the average seasonal temperature and precipitation dynamics, as well as their interannual variability, the spring campaign faced typical wet conditions (Table 2). The summer campaign faced specifically dry conditions with a mean temperature above and a mean precipitation below the normal range. Conditions before the autumn campaign tended to be wet and cold but were within the typical range.

Image Analysis

We developed a semiautomated image-processing scheme to derive quantitative measures of the biopore topology, biopore–matrix interaction, and infiltration patterns from the photographs of the horizontal layers. Image processing was performed with the following steps applied to each image: (i) image preparation by rectification, trimming, and blue channel adaption (Fig. 3a); (ii) image binarization and extraction of stained patches and biopores (Fig. 3b); (iii) visual check of the detected structures; and finally, (iv) image analysis of the binarized objects to evaluate the matrix interaction and the topology of detected biopores (Fig. 3c).

The basic functioning of structure identification by image binarization (Step ii) is explained in the paragraph below. A more comprehensive description of the individual processing steps (i–iv) can be found in the appendix.

We identified and labeled dye-stained patterns according to Jackisch (2015) by calculating the contrast between the green and blue channel of the input image. Afterward, a Sobel operator was applied on the binary image of stained pixels for edge detection of stained patches, followed by a watershed segmentation to break down large patches. We extended this method to additionally detect and label biopores. The crucial steps of the biopore binarization are image conversion into HSV (hue, saturation, and value) color space, morphological reconstruction by erosion to identify darker regions of the image surrounded by pixels of brighter values (i.e., biopores), and a downstream size and contrast filtering to isolate biopores. Since soil cracks occurred in most images of the summer campaign, their specific distinction from biopores was necessary. We extended the image processing by a crack detection routine to label cracks and to ensure a proper separation between biopores and cracks during image binarization of these four images. The crucial steps of the crack binarization are contrast enhancement of the greyscale image to emphasize cracks, crack separation by threshold filtering of the greyscale values, morphological opening to improve cracks' shape, and additional downstream size filtering to isolate cracks. Unless stated otherwise, all analyses were performed using Python 3.5 within the Anaconda distribution and IPython Notebook 4.0 (Perez and Granger, 2007). The main tools used for image processing originate from the library scikit-image (van der Walt et al., 2014).

Table 2. Mean temperature and precipitation for previous years vs. the year of investigation to characterize pre-experimental meteorological conditions. Values for 2005 to 2014 are given as monthly mean values with the SD of all mean values in parentheses to characterize the interannual variability. Values for 2015 are averages for the 30 d before of each measurement campaign. Data were obtained from the weather station in Useldange.

	2005–2014		2015	
Month	Temperature	Precipitation	Temperature	Precipitation
	°C	mm	°C	mm
April	9.9 (± 2.0)	41.0 (± 30.4)	9.5	50.2
June	17.0 (± 1.0)	74.6 (± 34.1)	18.4	32.7
September	14.4 (± 1.6)	53.6 (± 26.8)	12.4	76.5

Extending Dye Experiments with Numerical Simulations

Our aim with modeling was to extend the dye experiments in a temporal dimension and to use the model to investigate effects of different biopore setups on the development of infiltration patterns. We therefore used the nonuniform flow model echoRD to simulate the dye experiments.

Model Description

A comprehensive description of the echoRD model, including its testing and validation, is given by Jackisch and Zehe (2017). The model represents the soil matrix as a two-dimensional domain with representative one-dimensional vertical macropores. The concept uses a Lagrangian stochastic–physical framework to simulate the movement of single water particles. The diffusive particle movement in the matrix is simulated by means of a spatially explicit random walk, whereby the diffusivity depends on the soil water particle density using soil water retention properties parameterized through laboratory-derived van Genuchten parameters (Zehe and Jackisch, 2016). Advective flow in the macropores is simulated as film flow, self-controlled by interaction with the soil matrix. Therefore, the initial advective momentum is set to a maximum value, following the values for biopores in Shipitalo and Butt (1999), in our case. It is then retarded by friction at the pore wall, depending on the soil matric head of the surrounding matrix and pore network configuration. As such, the model overcomes the necessity of unobservable effective interaction parameters.

The echoRD model requires definition of the water retention properties of the soil matrix (Mualem–van Genuchten parameters and saturated hydraulic conductivity) and a distribution of macropore distances and diameters in different depth levels. It is driven by an initial soil moisture and a precipitation time series. Because echoRD is an event model, evapotranspiration is neglected.

Model Application

We simulated the irrigation experiments for one plot per season. The criterion of our plot selection was a biopore number similar to the median biopore number of the respective measurement campaign. We based our model setups on laboratory-derived

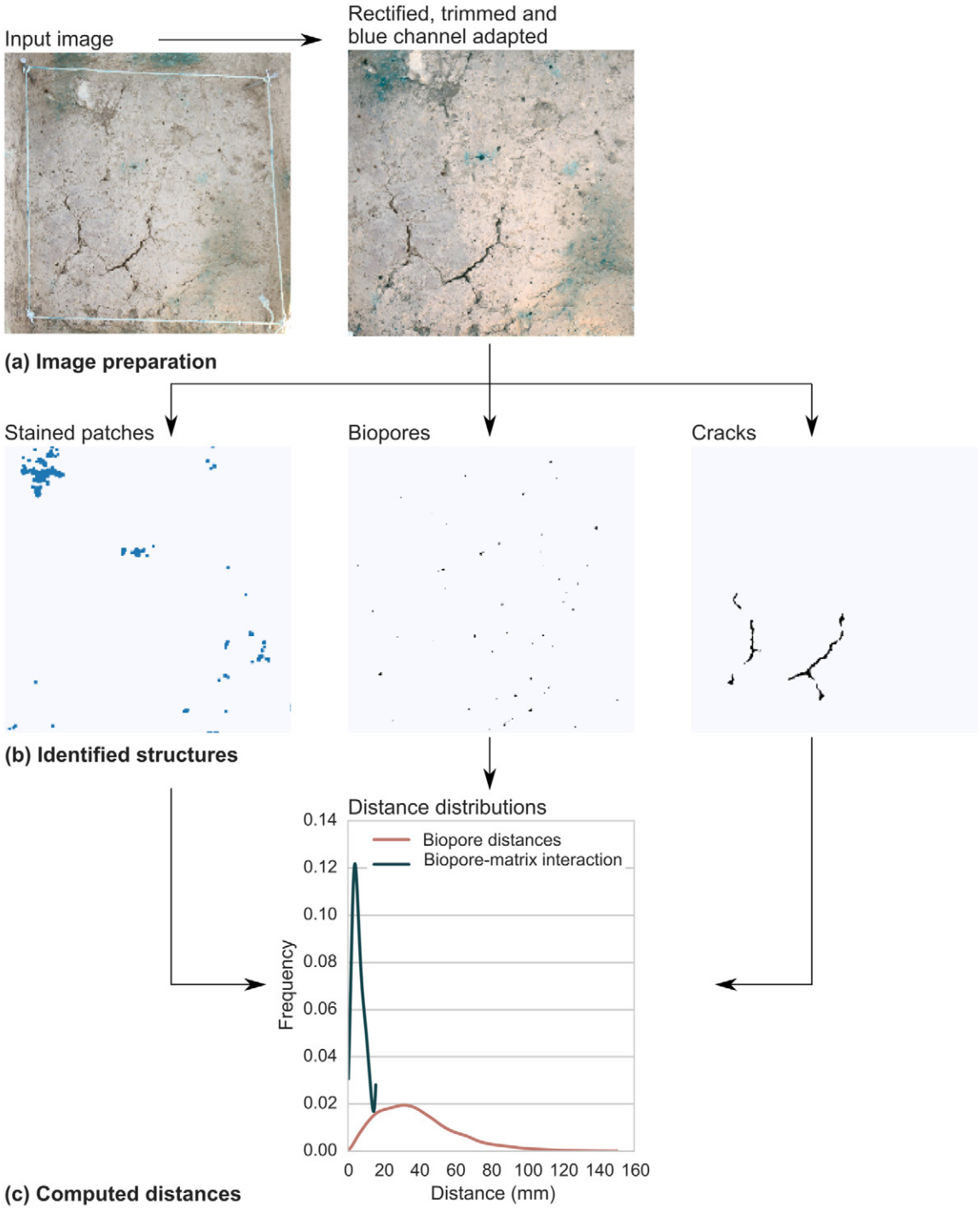

Fig. 3. Workflow of image processing with (a) realized image preparation steps, (b) the identified structures, and (c) exemplary output.

soil properties (Table 1), experimentally derived macropore definitions, and observed antecedent soil moisture conditions. As the exact irrigation rate is unknown for the different experiments, we decided to use a fixed irrigation supply of 40 mm in 30 min for each simulation. A detailed sensitivity analysis of the inflow rate in echoRD was provided by Jackisch and Zehe (2017).

In addition to numerical reproduction of the experiments, we built nine scenarios by shuffling all possible combinations of observed antecedent moisture conditions (a = spring, b = summer, and c = autumn) and macropore setups (A = spring, B = summer, and C = autumn; Fig. 4).Using this nomenclature, each modeling scenario is described in the text by a combination of two letters—a capital letter abbreviating the macropore setup, and a lowercase letter describing the initial soil moisture. Each modeling scenario was simulated for 24 h, except the scenarios with very high antecedent moisture values in spring, where simulation was limited

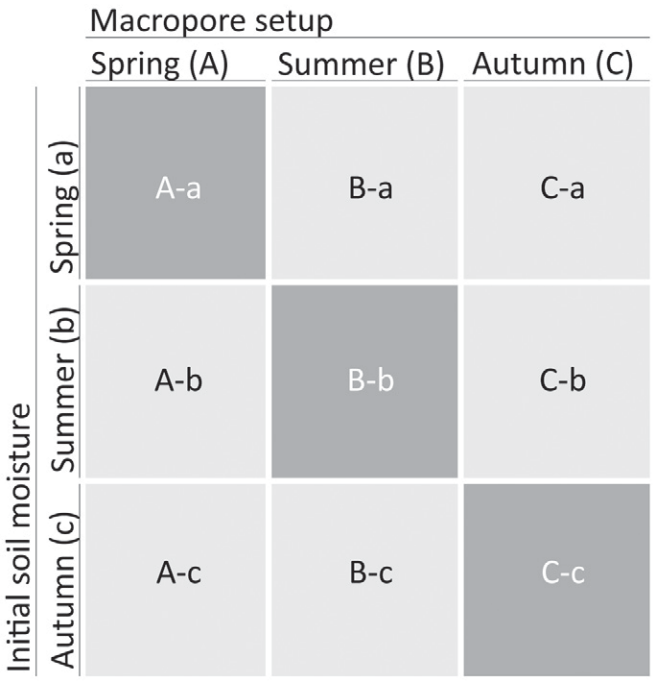

Fig. 4. Different runs of echoRD (ecohydrological particle model based on representative domains) using all possible combinations of macropore setups and initial soil moisture. The runs in the dark boxes are model scenarios in line with the respective field conditions determined per measurement campaign. The abbreviations for each box are used as run names within the text.

to 30 min due to high computation times. To assess the model output of each scenario, we compared the simulated infiltration profiles with the observed Brilliant Blue profiles. In a first step, we compared the three model scenarios in line with the respective field conditions per measurement (Scenarios A-a, B-b, and C-c; Fig. 4) to assess whether echoRD is capable of reproducing our infiltration experiments. In a second step, the effect of the temporally dynamic macropore settings was examined in the shuffled scenarios (A-b, A-c, B-a, B-c, C-a, and C-b; Fig. 4). We compared our Brilliant Blue profiles with the simulated infiltration profiles after 120 min, because Brilliant Blue adsorbs to soil material (Flury and Flühler, 1995). Moreover, Jackisch and Zehe (2017) showed that the infiltrations patterns stabilize quickly after the end of the event. This is in line with Germann and Karlen (2016), who argued that film flow inside macropores is totally absorbed into the soil matrix after 1.5 times the duration of water input. The paragraphs below describe in more detail how we parameterized the macropore domain and the hydraulic properties of the soil matrix, as well as how we specified the initial conditions.

To parameterize the macropore domain, we derived the distance distributions of effective biopores from the soil profiles (Fig. 5a; for more information regarding the distance calculation, see the appendix). The skewed distance distributions were square root transformed to obtain the required mean and SD as input. Internally, echoRD transforms the input back before setting up the macropore domain. Within the measurement campaigns, we only examined the upper 30 cm. Since the experiments did not cover depths below 30 cm, but biopores extend to greater depth, we used one horizontal image from an earlier irrigation experiment conducted with a comparable methodology (Brilliant Blue concentration of 4 g L^{-1}, irrigation intensity of 50 mm h^{-1}, horizontal excavation after 24 h) within the same study area (Jackisch, 2015) to complement the data basis. We assumed that biopore networks are more stable in greater depths. To obtain the required model input of biopore diameter distributions in different depths, we assigned an average size value for each size class (1.5 mm for <2 mm, 3.5 mm for 2–6 mm, 6.5 mm for >6 mm) (Fig. 5a). Figure 5b illustrates one possible realization of an effective macropore domain per measurement campaign. In spring and summer, the macropore domains host few but mostly continuous macropores due to similar distance distributions in the upper 30 cm. In autumn, the macropore domain hosts more macropores, with many macropores terminating at a depth of 10 cm, since the macropore distances clearly increase with depth.

For the moisture setups in spring and autumn, initial soil moisture for the upper 30 cm was defined according to measurements during the campaigns. Below 30 cm, as well as for the whole summer setup, moisture data from a neighboring hydrometeorological monitoring station (Zehe et al., 2014) was taken. In spring, the initial soil moisture was near saturation with ~0.42 cm^3 cm^{-3}, whereas in summer, the initial soil moisture was extremely low with ~0.15 cm^3 cm^{-3} (Table 3). In autumn, the initial soil moisture was between both extremes and ranged from 0.18 cm^3 cm^{-3} in the upper soil centimeter to 0.40 cm^3 cm^{-3} at the intermediate depth.

Results

Biopore Numbers

The distribution of manually counted biopore numbers varies clearly across the different sampling campaigns (Fig. 6). Overall, the total biopore numbers ranged from 32 to 392 pores m^{-2}. The largest number of effective biopores was recorded in autumn (352) and the smallest number in summer (12), both at a depth of 3 cm. In autumn, the difference between median total and effective pores was smallest. In spring and autumn, the total number of biopores decreased with depth. Furthermore, in spring and autumn, the fraction of effective biopores remained the same with depth, but not in summer. In summer, the total biopore number increased with depth, whereas the number of effective biopores remained low and constant with depth.

Biopore–Matrix Interaction

The distance of each stained pixel to the nearest stained biopore (Fig. 7) was used as an indicator for biopore–matrix interaction. In all sampling campaigns, the median biopore–matrix interaction was similar at the 3-cm depth. This interaction decreased with depth, especially in spring and autumn. In summer, the interaction remained relatively high, even at the lowest examined depth. Biopore–matrix interaction and antecedent soil

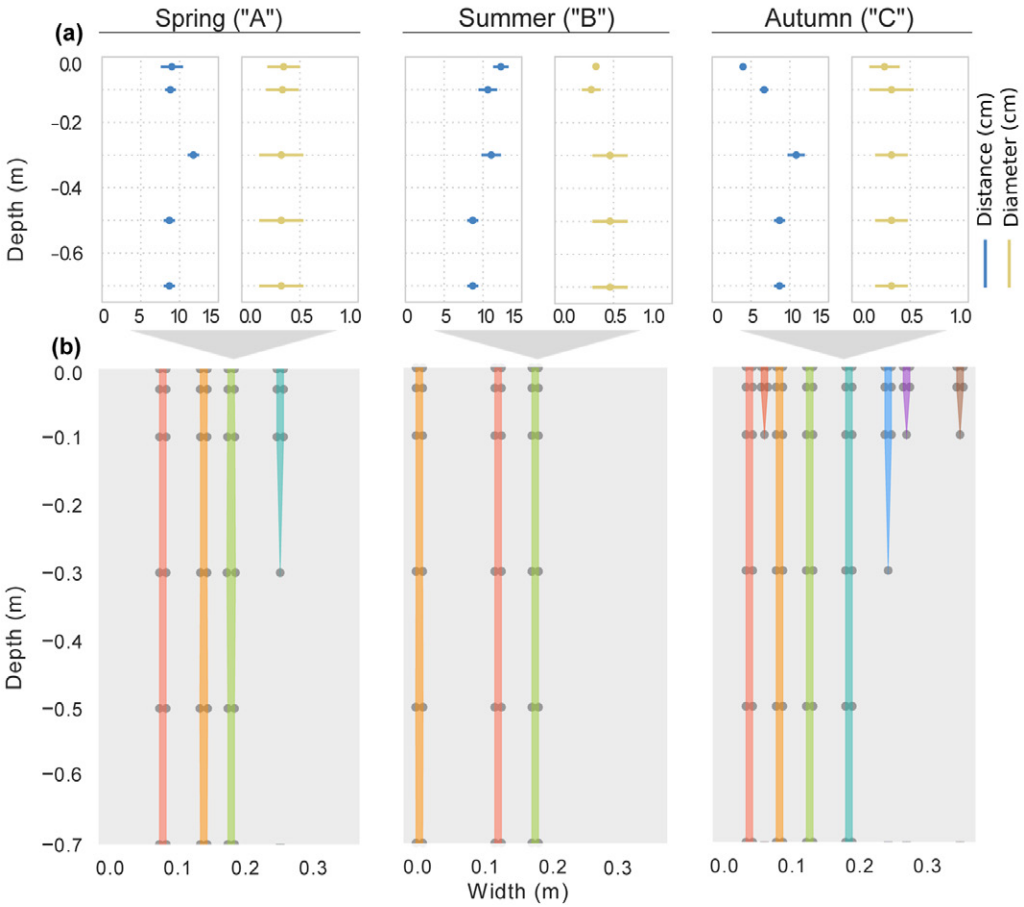

Fig. 5. (a) Image-derived distance distributions and field-derived diameter distributions of effective biopores used for parameterizing the macropore domain. The parenthesized letters represent the respective setup abbreviation. (b) One possible realization of the representative macropore domain for each measurement campaign. The macropore width represents the contact interface with the soil matrix.

Table 3. Initial volumetric soil moisture of each moisture setup used for modeling. The depth intervals of initial moistures are based on the representative depth of measurement. The parenthesized letters represent the respective setup abbreviation.

	Antecedent soil moisture		
Depth	Spring ("a")	Summer ("b")	Autumn ("c")
cm	——— $cm^3\ cm^{-3}$ ———		
0–5	0.45	0.14	0.18
5–20	0.41	0.14	0.34
20–40	0.43	0.16	0.40
40–70	0.40	0.17	0.27

moisture were significantly negatively correlated (Fig. 8). Only in spring and summer, four interaction values at depths of 3 cm (unfilled squares in Fig. 8) were higher than values from the same depth and season, despite similar moisture. We excluded these values when calculating the regression because we assumed that the homogeneous infiltration front in the soil matrix had already passed this depth. Hence, these four calculated distance values could not be attributed to biopore–matrix interaction primarily, which justified their omission as erroneous values.

Dye-Stained Patterns

The smallest stained area was observed in the horizontal images from spring (Fig. 9). In this campaign, the binary values of recovered Brilliant Blue strongly decreased between depths of 3

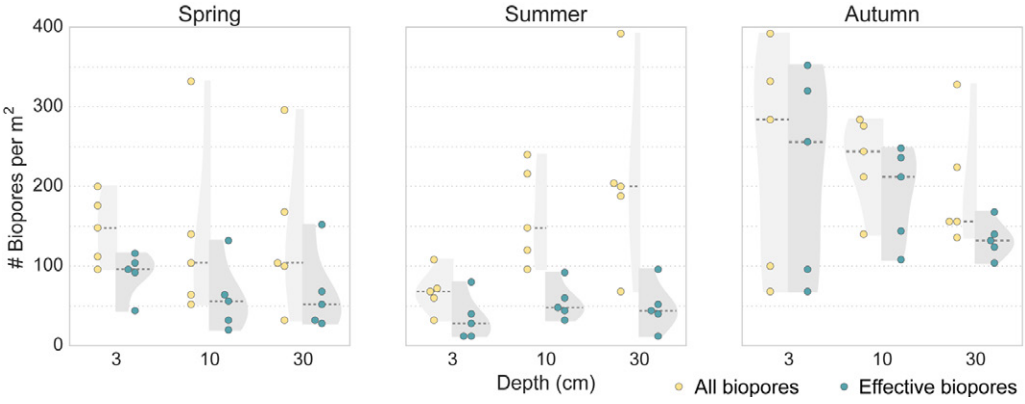

Fig. 6. Biopore counts per square meter. The term "effective biopore" relates to stained pores and, thus, flow participation. The deposited gray violins display a fitted kernel density estimate with a dotted line indicating the median per violin side.

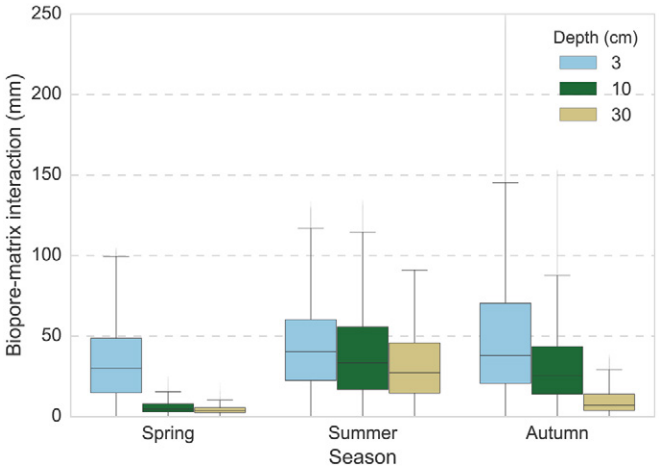

Fig. 7. Magnitude of biopore–matrix interaction presented as binary values of Brilliant Blue extension around effective biopores. Each boxplot contains distance values of five images.

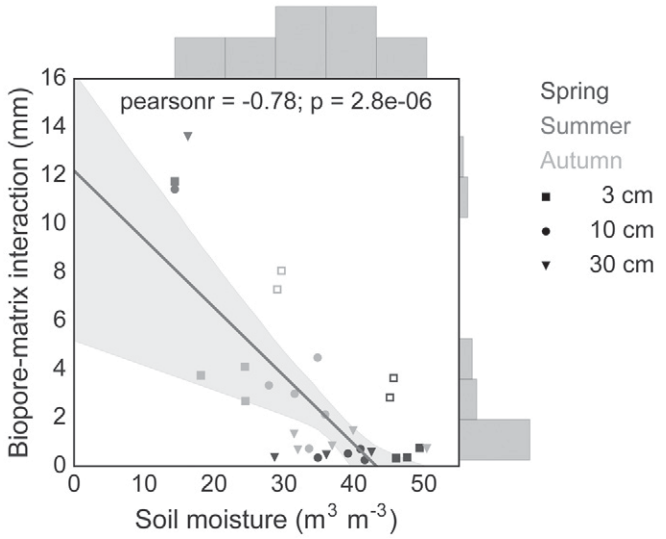

Fig. 8. Relationship between biopore–matrix interaction and soil moisture with regression line and deposited kernel density fit. The volumetric soil moisture are depth-wise average field measurements. To substitute missing moisture records in summer, values from a neighboring moisture measurement are taken and plotted against the depth-wise summed and averaged distances. The four unfilled square dots were excluded from calculating the regression because we regard these values as outliers due to measurement errors.

and 10 cm toward a dye coverage <2%. Especially in spring, it was remarkable how little the fraction of the stained area varied below a depth of 3 cm. Plots examined in autumn showed a similarly steep decrease of Brilliant Blue coverage below surface, but the magnitude of dye coverage was more than twice as high as the coverage in spring. Especially at the 3-cm depth, about half of the profile surface in autumn was stained, on average, and total staining ranged up to 80%. Only at the 30-cm depth, the low variance of dye coverage in autumn was similar to that in spring, but the mean Brilliant Blue coverage of 3.8% was still twice as high compared with spring. In summer, the course of stained area decreased almost linearly with depth. At a depth of 30 cm, dye coverage in summer was highest compared with spring and autumn, which coincided with the high biopore–matrix interaction observed there (Fig. 7).

Simulated Infiltration

The model simulations show clear preferential flow in macropores (Fig. 10). After 10 min of simulated infiltration, spring preferential flow reached twice the depth of that in summer or autumn. After the end of irrigation (30 min, Fig. 10), the simulated results of the three campaigns differed. The depth of preferential flow was 70, 50, and 40 cm in spring, summer, and autumn, respectively. The diffusive infiltration at the soil surface was limited to the top centimeters in spring and summer and reached depths of 10 cm in autumn. Between 30 and 60 min, the maximum infiltration depth changed marginally in all simulation scenarios, indicating that preferential flow stopped immediately after irrigation. From this point forward, the model output suggests that water fluxes were mainly diffusive water redistribution processes.

The simulated moisture distributions reflected important characteristics of the observed preferential flow patterns (rightmost column in Fig. 10). For spring and summer, the modeling results showed diffusive infiltration strictly limited to the top centimeter within the profile, and lateral infiltration played a minor role in spring but a major role in summer. However, in autumn, the particle numbers at the intermediate depth were overestimated compared with the observed Brilliant Blue patches, probably because not all field-recorded shallow biopores actually ended at a depth of 10 cm, as assumed in the model. Nonetheless, the strong diffusive infiltration in the soil surface and the strong decrease of dye coverage toward a depth of 30 cm was well reflected in the model output.

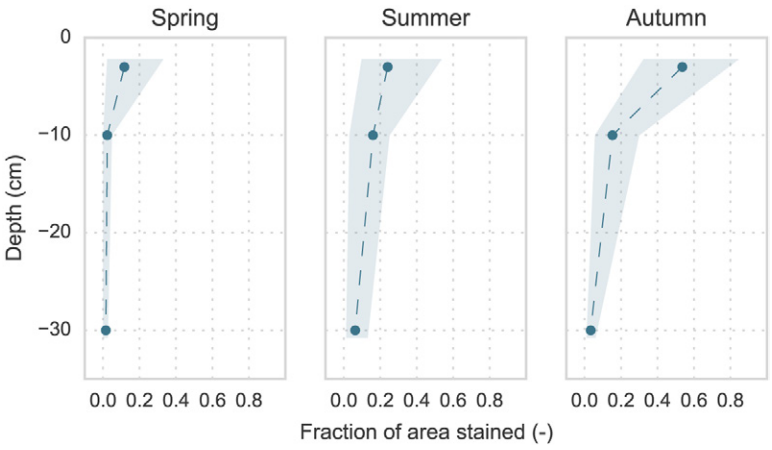

Fig. 9. Depth profiles of stained areas. Each point represents the mean of the stained fraction for each depth and month, with the deposited range indicated by the blue background.

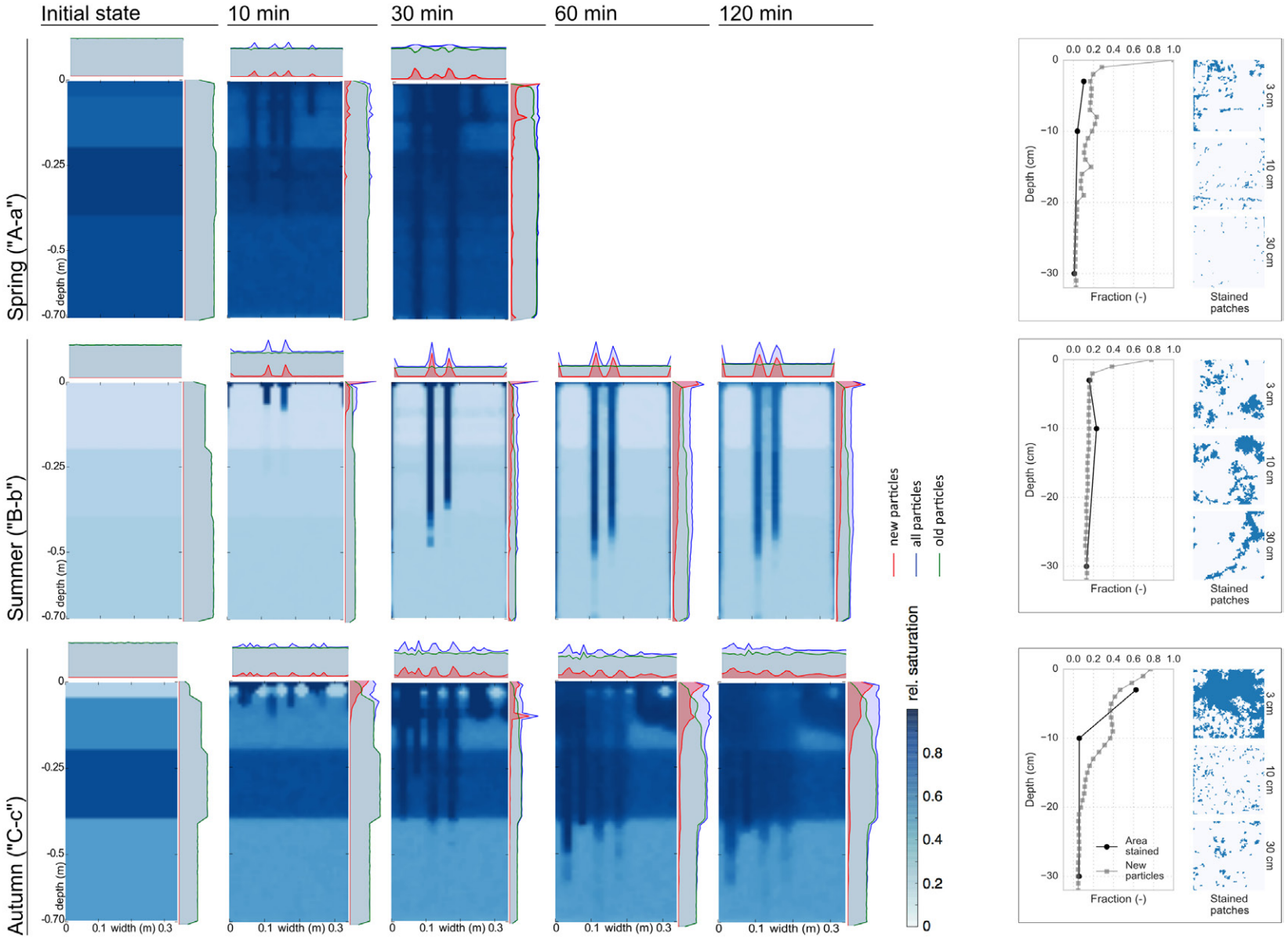

Fig. 10. Results of modeling experiments in line with the respective field conditions per measurement campaign (see Fig. 4 for abbreviated scenario names). Soil moisture is displayed as relative saturation (rel. saturation). The marginal plots show the lateral and vertical distributions of old (initial state), new (input through upper boundary), and all particles. Vertical Brilliant Blue distributions and horizontal dye patterns observed in the field are shown on the right side of the figure. The modeling scenario in spring was only computed for 30 min due to high computation times. The deposited particle distribution is all the new particles summed at the time of 30 (in the first row) or 120 min (in the second and third rows) and then normalized by the maximum possible number of particles per grid cell (determined by porosity).

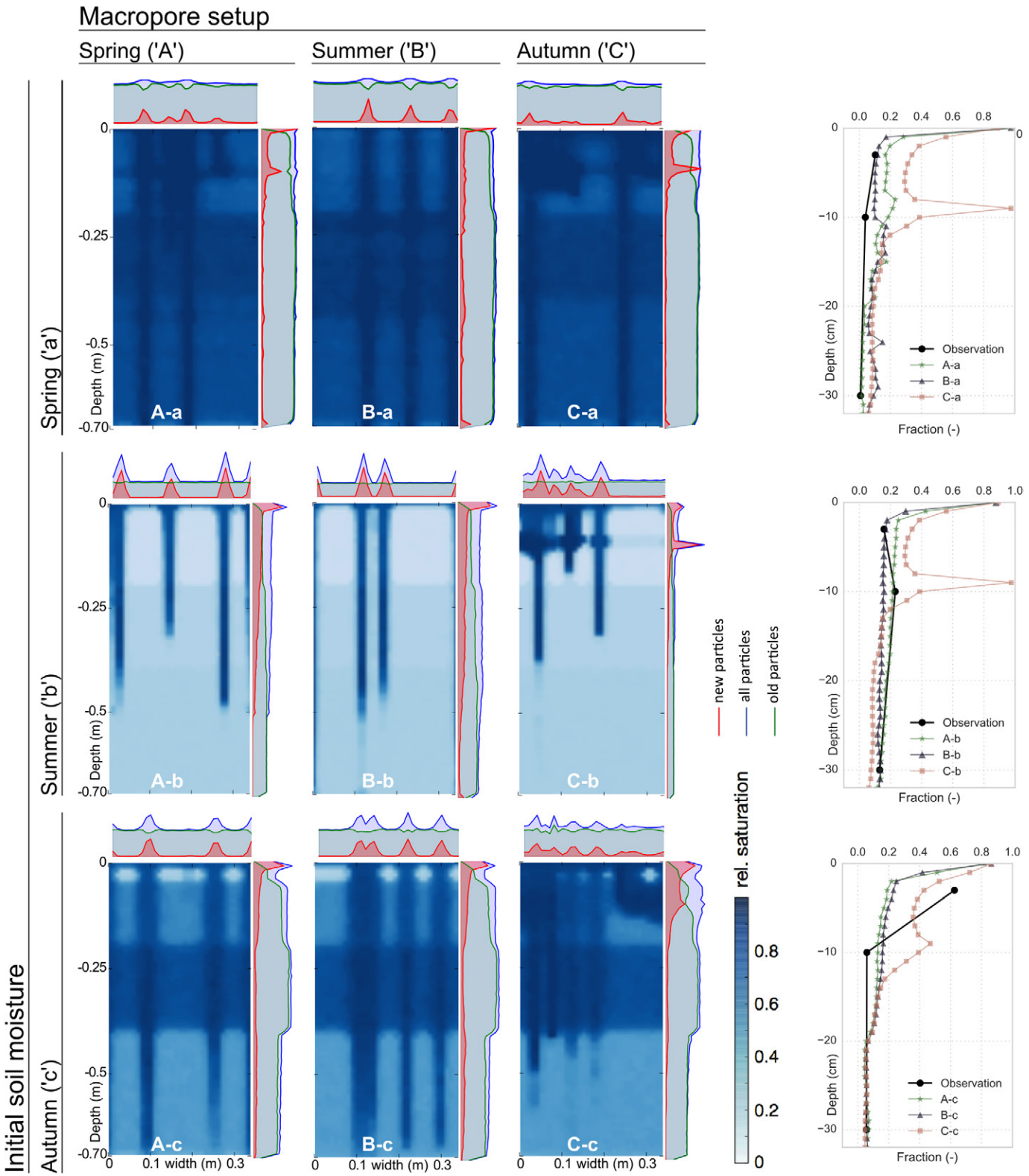

Fig. 11. Moisture distributions simulated for all combinations of initial soil moisture and macropore setup at the time of 30 (first row) and 60 min (second and third row). Soil moisture is displayed as relative saturation (rel. saturation). The modeling results on the diagonal from the upper left to the lower right are congruent to field conditions during the measurement campaigns. The setup combinations are displayed at the bottom of each subplot (see Fig. 4 for abbreviations). The observed and simulated infiltration profiles are displayed beside the modeling results. Note that the particle distribution is all the new particles summed at the time of 30 or 60 min and then normalized by the maximum possible number of particles per grid cell (determined by porosity). The observed infiltration profiles are the depth profiles of Brilliant Blue coverage.

The comparison of all possible setup combinations demonstrates that, in addition to initial soil moisture, the spatial distribution of biopores substantially influence the simulated infiltration patterns (Fig. 11). Generally, macropore setups generated with observed distance distributions from spring and summer are more similar than those from autumn (Fig. 5). Consequently, the interchange of spring with summer biopores changed the simulated infiltration profile in the upper 30 cm to only a minor extent, and both setups match our observations equally well (check A-a and B-a, as well as A-b and B-b, against the observations in Fig. 11). By contrast, using the macropore setups generated with distance distributions from autumn for the spring and summer situations changed the infiltration profile to a major extent (rightmost column in Fig. 11). Coupling the autumn biopores with moisture values from spring or summer generated infiltration profiles clearly disagreeing with the observed Brilliant Blue profiles because of largely overestimated moisture changes up to a depth of 10 cm due to many shallow biopores (Fig. 5, check C-a and C-b against observations in Fig. 11). Moreover, coupling the spring or summer macropore setups with autumn moisture also generated infiltration profiles disagreeing with observed Brilliant Blue profiles because of an underestimated diffusive infiltration up to a depth of 10 cm (check A-c and B-c against observations in Fig. 11).

Discussion

Biopore Numbers

Both the range and the high variability of biopore numbers are comparable with results from other studies; our field-recorded biopore numbers ranged from 32 to 392 counts m^{-2}, which is similar to the findings of van Schaik et al. (2013) with 24 to 308 counts m^{-2}, but higher than the findings of Zehe et al. (2001) with 90 to 250 counts m^{-2} and lower than the findings of Pérès et al. (2010) with 395 to 592 counts m^{-2}. All studies were conducted in a catchment with comparable climatological settings. Except for the intermediate depth in Pérès et al. (2010), all studies exhibited decreasing biopore numbers with depth, which agrees with our results, but only for the spring and autumn campaigns, probably because the reference studies were conducted in spring or autumn, respectively. By contrast, in summer, the increasing biopore numbers with depth agree with Ehlers (1975), who also observed decreasing biopore numbers with depth during summer measurements.

van Schaik et al. (2013) found a strong, linear relation between total and effective biopore numbers for different depths. Our data also indicated a linear relation of total and effective biopore numbers in spring and autumn. However, in summer, we did not observe such a relation, since the number of effective biopores was constant with depth, whereas the total biopore number increased. These findings suggest that temporally changing biopore numbers, mainly in the top soil centimeters, determine the fraction of the biopore network in which preferential flow occurred. Although not all field-recorded biopores are certainly attributed to earthworm activity, the temporally changing biopore numbers coincide with temporally changing earthworm numbers observed in the Attert catchment. For example, Schneider et al. (2017) found lowest earthworm numbers in July and a significantly higher prevalence of earthworms in autumn than in spring. Pagenkemper et al. (2015) demonstrated that earthworm activity not only means newly drilled pores, but also pore network modifications such as interconnecting branches of their burrows. Furthermore, it is known that earthworms seal their burrows or migrate deeper (Lavelle, 1988) and become inactive to persist in unfavorable conditions (Eggleton et al., 2009), a fact that was confirmed by several dormant earthworms found in our summer campaign.

Biopore Dynamics and Infiltration Patterns

Preferential flow in macropores occurred in all measurement campaigns, since dye staining extended in all plots up to depths of 30 cm. The large variation in infiltration patterns is similar to findings from other studies (Weiler and Naef, 2003; Weiler and Flühler, 2004; Cey and Rudolph, 2009; van Schaik, 2009; van Schaik et al., 2013). However, studies quantifying the magnitude of biopore–matrix interaction are scarce. Weiler and Flühler (2004) measured interaction values mainly concentrated around distances of 10 to 20 mm, which correspond well with our findings from summer and autumn. In spring, biopore–matrix interaction was lower, with values between 5 and 10 mm in the two deeper examined depths. The correlation between biopore–matrix interaction and soil moisture confirms the major influence of soil moisture on the transfer of water from macropores into the bulk soil, found by Weiler and Naef (2003). Continuing from this, we focus on the comparison between the three measurement campaigns to emphasize the effect of biopore temporal dynamics on infiltration patterns.

In spring, dye coverage and biopore–matrix interaction were lowest. Hence, the majority of irrigated water must have bypassed the examined profiles. Such significant macropore flow is initiated by saturated soil layers (Weiler and Naef, 2003). We observed high antecedent soil moisture near saturation in spring up to a depth of 3 cm (0.42 cm^3 cm^{-3}). Moreover, significant macropore flow occurs as film or rivulet flow with high velocities (Cey and Rudolph, 2009) when the supply of water to macropores is high or when the interaction is low. Interaction can be reduced by biopore wall coatings (Jégou et al., 2001). In line with Weiler (2005), the most probable cause for the low interaction in spring is a combination of both: significant macropore flow with high advective velocities and coating of the biopore walls. Additionally, lateral infiltration into the soil matrix was rather limited along the pore walls due to the nearly water-saturated bulk soil.

In summer, macropore flow with high interaction occurred in all three examined depths. Dry soil conditions (0.15 cm^3 cm^{-3}) were the main causes for the high interaction because of increased water suction into the bulk soil. In addition, soil drought favored compaction fissures and cracks. In some of the deeper profiles, infiltration into cracks was observed. Because we found similar numbers of effective biopores in all three depths, we assumed

continuous pores throughout our examined profiles, rather than dead-ending pores. Thus, lateral water diffusion must have taken place mainly during flow conditions, and changed biopore wall properties might have favored the increased interaction in summer. Zangerlé et al. (2014) demonstrated a sharp decrease (around a third) of total C and N contents of internal earthworm casts within 2 or 3 d after earthworm removal from culture boxes. The organic matter of intact walls of earthworm burrows shows an especially decreased potential wettability (Leue et al., 2015) and thus impedes lateral mass exchange. Hence, earthworm aestivation suggests a decrease of biopore coatings in summer and may be another reason for the increased infiltration from biopores into the bulk soil.

In autumn, we observed diffusive infiltration at the 3-cm depth, macropore flow with moderate interaction at the 10-cm depth, and macropore flow with low interaction at the 30-cm depth. The diffusive flow at the 3-cm depth coincided with the significantly higher biopore amount recorded there. The strong decrease of effective biopores below depths of 3 cm implied many dead-ending biopores, which reflected the observed decline of dye coverage with depth. Thus, accumulated water inside ending pores was redistributed to the bulk soil. This process enhances lateral infiltration from biopores (Cey and Rudolph, 2009) and explains the high interaction observed for the two upper horizontal profiles in autumn. A lot of irrigated water became stored in the upper soil due to the high diffusive infiltration. This point raises the question of how much water passed through pores at the depths of 10 and 30 cm. The low interaction might lead to the conclusion that there was low macropore flow in deeper profiles, but, similar to the spring situation, exchange could have also been impeded due to increased pore wall coatings because of high earthworm activity and high antecedent soil moisture below depths of 10 cm (0.40 cm^3 cm^{-3}).

Simulated Infiltration

Our modeling objective was a qualitative reproduction of the characteristic type of the nonuniform infiltration patterns observed per measurement campaign. This objective was accomplished, since the model was capable to reproduce (i) significant macropore flow with low interaction in spring, (ii) macropore flow with high interaction in all examined depths in summer, and (iii) macropore flow with high interaction in the top centimeters of soil in autumn. In a quantitative comparison (rightmost column in Fig. 10), the virtually reproduced infiltration profiles do not perfectly match their respective Brilliant Blue profiles. A perfect match between both was not our intended goal, since Brilliant Blue is not suitable as a quantitative validation reference, mostly because its dispersion is biased toward higher flow velocities and its explanatory power regarding water flow is limited to a qualitative visualization of the respective flow paths (Flury and Flühler, 1995). However, the simulation results from all possible setup combinations reinforce our perception from field experiments that, in additional to antecedent soil moisture, temporal biopore dynamics affect infiltration patterns, although with some reservations, which are discussed below.

A clear influence of temporally changing biopore numbers on infiltration can be seen only when interchanging the macropore setups spring and autumn or summer and autumn, but not when interchanging spring and summer. In the examined depths of 3, 10, and 30 cm, respectively, we counted effective biopore numbers of 80, 40, and 16 in spring; 20, 36, and 28 in summer; and 264, 72, and 36 in autumn on the plots used for setting up the macropore domain. Combining field experiments and modeling results allows two conclusions. Firstly, high biopore numbers (autumn) effect a major change in infiltration profiles compared with low (summer) or intermediate (spring) biopore numbers. Secondly, aside from the absolute biopore numbers, this fact is mainly attributable to the strong decrease of biopore numbers with depth in autumn (Fig. 5) and supports previous findings regarding the importance of biopore continuity in the context of preferential flow (Allaire-Leung et al., 2000a; Bastardie et al., 2003; Capowiez et al., 2014). Moreover, the latter conclusion suggests that more biopores do not necessarily increase the water drainage but also can increase the water storage of infiltrating water. Hence, our results support the call of Jarvis et al. (2016) to consider soil structures dynamically in preferential flow simulations. Measuring three biopore distributions at three different dates in 1 yr, we received a range of obviously differing infiltration profiles. Although we examined only three dates in 1 yr, it can be expected that biopore dynamics exist during the whole year, mostly because our three field experiments covered a wide range of weather conditions typically occurring during different seasons, and because of the proven influence of weather conditions on seasonally changing earthworm activity and abundance (Eggleton et al., 2009). However, further measurements are needed to confirm whether our findings reflect the seasonal dynamics of biopores and to identify the influencing factors of these dynamics.

Conclusion

The present study examined temporal changes in biopore networks and the resulting infiltration patterns. Therefore, we (i) conducted irrigation experiments with Brilliant Blue, (ii) analyzed the emerging dye patterns in the soil using a semiautomated image-processing scheme, and (iii) extended the field experiments with numerical simulations.

According to the field records, we proved that biopore numbers and the structure of an effective biopore network can differ substantially over time. An important consequence is that different processes dominate water infiltration in different measurement campaigns. In spring, we observed the smallest stained area because most of the infiltrating water bypassed our examined profiles due to moderate biopore numbers in combination with limited matrix interaction due to matrix saturation. In summer, we observed few but extended preferential flow patterns up to the lowest considered depth of 30 cm due to small numbers of effective

biopores but strong matrix interaction. In autumn, we observed a high diffusive infiltration in the upper soil centimeter due to many dead-ending biopores. Thus, most of the infiltrating water was retained within the examined profile.

The simulated scenarios confirmed the necessity to include temporally varying effective biopore networks. Additionally, the simulation experiments confirmed the well-known influence of soil moisture on macropore flow. However, further research is required to assess our deduced hypothesis that changes in biopore wall properties additionally influenced the observed variations in infiltrations. Nonetheless, our results provide strong evidence for the need to consider temporal biopore dynamics in preferential flow simulations. This is especially the case, if a realistic representation of soil water flow processes is needed, for instance, when considering mass transfer and turnover processes in biopores, notably in terms of leaching plant protection products and nutrients toward the groundwater body.

Appendix

Prior to the actual image analysis, some preparatory steps were performed to receive comparable results by image processing (Fig. 3a). To compensate lens distortion and off-centered photographs, a rectification was performed using the perspective transformation tool from OpenCV (the Open Source Computer Vision library). Simultaneously, each image was trimmed to 50 × 50 cm^2 to ensure the same scaling for all pictures. The resulting image size was 500 × 500 pixels, with each pixel representing an area of 1 mm^2. Pictures with shadings caused by stones or edge regions, for example, required a local contrast enhancement to improve the detection accuracy of biopores. Furthermore, a blue channel adjustment via gradation adaption was conducted for a consistent identification of stained patches. Both tasks were executed with Adobe Photoshop 5.5.

Most image analysis tools used in this study were taken from the Python package scikit-image (van der Walt et al., 2014) for image processing and from the Python package NumPy (Oliphant, 2007) for general calculations. A downhill filter algorithm suppressing light regions in the image while keeping darker spots (Robinson and Whelan, 2004) was used for morphological reconstruction to extract biopores from the image. The received image of dark spots was first roughly filtered for biopore-like structures by histogram thresholding and was then further filtered by black spots' size. This size filtering ensured the exclusion of small objects caused by loose soil particles, roots, or surface unevenness. For crack detection, a contrast enhancement was used. By default, this contrast amplification was limited to values within a given percentile of dark image values to emphasize cracks only. A sequence of morphological erosion and dilation was implemented to improve the crack morphology by connecting neighboring crack fractions and removing white pixels within cracks. Finally, the segregation of cracks from noise was performed by size filtering. All steps required a threshold definition. Because of differing light conditions between all images, these thresholds required an adjustment by visually inspecting the recovery of recorded biopores.

The identified biopores and stained patches (Fig. 3b) were concatenated to distinguish between stained (effective biopores) and unstained biopores. For the effective biopores, the network topology was calculated following Weiler and Flühler (2004). Therefore, the Euclidian distance of each image pixel to the nearest biopore was calculated as a proxy for their spatial arrangement in relation to the soil matrix. Furthermore, the distance of each stained image pixel to the nearest effective biopore was calculated as a proxy for the matrix–biopore interaction (Fig. 3c). Both steps were computed using the kd-tree algorithm for nearest-neighbor lookup (Maneewongvatana and Mount, 1999) from the Python package SciPy (Oliphant, 2007). All codes used for the image analysis can be accessed on GitHub (https://github.com/arneck).

Acknowledgments

We thank Theresa Blume and Tobias Vetter for providing soil moisture data from the sensor cluster in the Catchments as Organised Systems (CAOS) monitoring network. We especially thank the farmer Mario Kleer for providing access to the pasture. Furthermore, we would like to thank the two anonymous reviewers and the editor for their valuable comments and suggestions. This study is part of the Deutsche Forschungsgemeinschaft-funded CAOS project "From Catchments as Organised Systems to Models based on Dynamic Functional Units" (FOR 1598 SCHA1719/1-2 and SCHR1000/6-2).

References

Allaire-Leung, S., S. Gupta, and J. Moncrief. 2000a. Water and solute movement in soil as influenced by macropore characteristics: 1. Macropore continuity. J. Contam. Hydrol. 41:283–301. doi:10.1016/S0169-7722(99)00079-0

Allaire-Leung, S., S. Gupta, and J. Moncrief. 2000b. Water and solute movement in soil as influenced by macropore characteristics: 2. Macropore tortuosity. J. Contam. Hydrol. 41:303–315. doi:10.1016/S0169-7722(99)00074-1

Allroggen, N., N.L.M.B. van Schaik, and J. Tronicke. 2015. 4D ground-penetrating radar during a plot scale dye tracer experiment. J. Appl. Geophys. 118:139–144. doi:10.1016/j.jappgeo.2015.04.016

Bastardie, F., Y. Capowiez, J.-R. de Dreuzy, and D. Cluzeau. 2003. X-ray tomographic and hydraulic characterization of burrowing by three earthworm species in repacked soil cores. Appl. Soil Ecol. 24:3–16. doi:10.1016/S0929-1393(03)00071-4

Bastardie, F., Y. Capowiez, P. Renault, and D. Cluzeau. 2005. A radio-labelled study of earthworm behaviour in artificial soil cores in term of ecological types. Biol. Fertil. Soils 41:320–327. doi:10.1007/s00374-005-0847-6

Beven, K., and P. Germann. 1982. Macropores and water flow in soils. Water Resour. Res. 18:1311–1325. doi:10.1029/wr018i005p01311

Beven, K., and P. Germann. 2013. Macropores and water flow in soils revisited. Water Resour. Res. 49:3071–3092. doi:10.1002/wrcr.20156

Blouin, M., M.E. Hodson, E.A. Delgado, G. Baker, L. Brussaard, K.R. Butt, et al. 2013. A review of earthworm impact on soil function and ecosystem services. Eur. J. Soil Sci. 64:161–182. doi:10.1111/ejss.12025

Bogner, C., B.T. Widemann, and H. Lange. 2013. Characterising flow patterns in soils by feature extraction and multiple consensus clustering. Ecol. Inform. 15:44–52. doi:10.1016/j.ecoinf.2013.03.001

Botschek, J., S. Krause, T. Abel, A. Skowronek. 2002. Hydrological parameterization of piping in loess-rich soils in the Bergisches Land, Nordrhein-Westfalen, Germany. J. Plant Nutr. Soil Sci. 165:506–510. doi:10.1002/1522-2624(200208)165:4<506::AID-JPLN506>3.0.CO;2-7

Bouma, J., and L.W. Dekker. 1978. A case study on infiltration into dry clay soil I. Morphological observation. Geoderma 20:27–40. doi:10.1016/0016-7061(78)90047-2

Capowiez, Y., S. Cadoux, P. Bouchant, S. Ruy, J. Roger-Estrade, G. Richard, and H. Boizard. 2009. The effect of tillage type and cropping system on earthworm communities, macroporosity and water infiltration. Soil Tillage Res. 105:209–216. doi:10.1016/j.still.2009.09.002

Capowiez, Y., P. Monestiez, and L. Belzunces. 2001. Burrow systems made by *Aporrectodea nocturna* and *Allolobophora chlorotica* in artificial cores: Morphological differences and effects of interspecific interactions. Appl. Soil Ecol. 16:109–120. doi:10.1016/S0929-1393(00)00110-4

Capowiez, Y., S. Sammertino, and E. Michel. 2014. Burrow systems of endogeic earthworms. Effects of earthworm abundance and consequence for soil water infiltration. Pedobiologia 57:303–309. doi:10.1016/j.pedobi.2014.04.001

Cey, E.E., and D.L. Rudolph. 2009. Field study of macropore flow processes using tension infiltration of a dye tracer in partially saturated soils. Hydrol. Processes 23:1768–1779. doi:10.1002/hyp.7302

Colbach, R. 2003. Carte géologiques détaillée, nouvelle ed., Feuille no. 7/Redange [geological map]. (In French.) Serv. Géol. Luxembourg, Bertrange. Scale 1:25,000.

Daniel, O., A. Kretschmar, Y. Capowiez, L. Kohli, and J. Zeyer. 1997. Computer-assisted tomography of macroporosity and its application to study the activity of the earthworm *Aporrectodea nocturna*. Eur. J. Soil Sci. 48:727–737. doi:10.1046/j.1365-2389.1997.00111.x

Deutsches Institut für Normung. 2002. DIN ISO 11277. Soil quality: Determination of particle size distribution in mineral soil material: Method by sieving and sedimentation. (ISO 11277: 1988, Corrigendum 1: 2002). Beuth Verlag, Berlin, Germany.

Eggleton, P., K. Inward, J. Smith, D.T. Jones, and E. Sherlock. 2009. A six year study of earthworm (*Lumbricidae*) populations in pasture woodland in southern England shows their responses to soil temperature and soil moisture. Soil Biol. Biochem. 41:1857–1865. doi:10.1016/j.soilbio.2009.06.007

Ehlers, W. 1975. Observations on earthworm channels and infiltration on tilled and untilled loess soil. Soil Sci. 119:242–249. doi:10.1097/00010694-197503000-00010

Faybishenko, B.A. 1995. Hydraulic behavior of quasi-saturated soils in the presence of entrapped air: Laboratory experiments. Water Resour. Res. 31:2421–2435. doi:10.1029/95WR01654

Felten, D., and C. Emmerling. 2009. Earthworm burrowing behaviour in 2D terraria with single- and multi-species assemblages. Biol. Fertil. Soils 45:789–797. doi:10.1007/s00374-009-0393-8

Flury, M., and H. Flühler. 1995. Tracer characteristics of Brilliant Blue FCF. Soil Sci. Soc. Am. J. 59:22–27. doi:10.2136/sssaj1995.03615995005900010003x

Gerke, H.H. 2006. Preferential flow descriptions for structured soils. J. Plant Nutr. Soil Sci. 169:382–400. doi:10.1002/jpln.200521955

Germann, P.F., and M. Karlen. 2016. Viscous-flow approach to in situ infiltration and in vitro saturated hydraulic conductivity determination. Vadose Zone J. 15(2). doi:10.2136/vzj2015.05.0065

IUSS Working Group WRB. 2015. World reference base for soil resources 2014. Update 2015. International soil classification system for naming soils and creating legends for soil maps. World Soil Resour. Rep. 106. FAO, Rome.

Jackisch, C. 2015. Linking structure and functioning of hydrological systems: How to achieve necessary experimental and model complexity with adequate effort. Ph.D. diss., Karlsruher Inst. Technol. (KIT), Karlsruhe, Germany. doi:10.5445/IR/1000051494

Jackisch, C., L. Angermann, N. Allroggen, M. Sprenger, T. Blume, J. Tronicke, and E. Zehe. 2017. Form and function in hillslope hydrology: In situ imaging and characterization of flow-relevant structures. Hydrol. Earth Syst. Sci. 21:3749–3775. doi:10.5194/hess-21-3749-2017

Jackisch, C., and E. Zehe. 2017. Ecohydrological particle model based on representative domains. Hydrol. Earth Syst. Sci. Discuss. doi:10.5194/hess-2017-676

Jarvis, N., J. Koestel, and M. Larsbo. 2016. Understanding preferential flow in the vadose zone: Recent advances and future prospects. Vadose Zone J. 15(12). doi:10.2136/vzj2016.09.0075

Jarvis, N.J. 2007. A review of non-equilibrium water flow and solute transport in soil macropores: Principles, controlling factors and consequences for water quality. Eur. J. Soil Sci. 58:523–546. doi:10.1111/j.1365-2389.2007.00915.x

Jarvis, N.J., and I. Messing. 1995. Near-saturated hydraulic conductivity in soils of contrasting texture measured by tension infiltrometers. Soil Sci. Soc. Am. J. 59:27–34. doi:10.2136/sssaj1995.03615995005900010004x

Jégou, D., S. Schrader, H. Diestel, and D. Cluzeau. 2001. Morphological, physical and biochemical characteristics of burrow walls formed by earthworms. Appl. Soil Ecol. 17:165–174. doi:10.1016/S0929-1393(00)00136-0

Klaus, J., E. Zehe, M. Elsner, C. Külls, and J.J. McDonnell. 2013. Macropore flow of old water revisited: Experimental insights from a tile-drained hillslope. Hydrol. Earth Syst. Sci. 17:103–118. doi:10.5194/hess-17-103-2013

Koestel, J., R. Kasteel, A. Kemna, O. Esser, M. Javaux, A. Binley, and H. Vereecken. 2009. Imaging Brilliant Blue stained soil by means of electrical resistivity tomography. Vadose Zone J. 8:963–975. doi:10.2136/vzj2008.0180

Koestel, J., and M. Larsbo. 2014. Imaging and quantification of preferential solute transport in soil macropores. Water Resour. Res. 50:4357–4378. doi:10.1002/2014WR015351

Köhne, J.M., S. Köhne, and J. Šimůnek. 2009. A review of model applications for structured soils: a) Water flow and tracer transport. J. Contam. Hydrol. 104:4–35. doi:10.1016/j.jconhyd.2008.10.002

Lavelle, P. 1988. Earthworm activities and the soil system. Biol. Fertil. Soils 6:237–251. doi:10.1007/BF00260820

Leue, M., H.H. Gerke, and R.H. Ellerbrock. 2013. Millimetre-scale distribution of organic matter composition at intact biopore and crack surfaces. Eur. J. Soil Sci. 64:757–769. doi:10.1111/ejss.12098

Leue, M., H.H. Gerke, and S.C. Godow. 2015. Droplet infiltration and organic matter composition of intact crack and biopore surfaces from clay-illuvial horizons. J. Plant Nutr. Soil Sci. 178:250–260. doi:10.1002/jpln.201400209

Luo, L., H. Lin, and P. Halleck. 2008. Quantifying soil structure and preferential flow in intact soil using X-ray computed tomography. Soil Sci. Soc. Am. J. 72:1058–1069. doi:10.2136/sssaj2007.0179

Maneewongvatana, S., and D.M. Mount. 1999. It's okay to be skinny, if your friends are fat. In: Proceedings of the Center for Geometric Computing 4th Annual Workshop on Computational Geometry, Baltimore, MD. 15–16 Oct. 1999. Univ. of Maryland, College Park.

Oliphant, T.E. 2007. Python for scientific computing. Comput. Sci. Eng. 9:10–20. doi:10.1109/MCSE.2007.58

Pagenkemper, S.K., M. Athmann, D. Uteau, T. Kautz, S. Peth, and R. Horn. 2015. The effect of earthworm activity on soil bioporosity: Investigated with X-ray computed tomography and endoscopy. Soil Tillage Res. 146:79–88. doi:10.1016/j.still.2014.05.007

Pelosi, C., G. Grandeau, and Y. Capowiez. 2017. Temporal dynamics of earthworm-related macroporosity in tilled and non-tilled cropping systems. Geoderma 289:169–177. doi:10.1016/j.geoderma.2016.12.005

Pérès, G., A. Bellido, P. Curmi, P. Marmonier, and D. Cluzeau. 2010. Relationships between earthworm communities and burrow numbers under different land use systems. Pedobiologia 54:37–44. doi:10.1016/j.pedobi.2010.08.006

Perez, F., and B.E. Granger. 2007. IPython: A system for interactive scientific computing. Comput. Sci. Eng. 9:21–29. doi:10.1109/MCSE.2007.53

Robinson, K., and P.F. Whelan. 2004. Efficient morphological reconstruction: A downhill filter. Pattern Recognit. Lett. 25:1759–1767. doi:10.1016/j.patrec.2004.07.002

Rogasik, H., S. Schrader, I. Onasch, J. Kiesel, and H.H. Gerke. 2014. Micro-scale dry bulk density variation around earthworm (*Lumbricus terrestris* L.) burrows based on X-ray computed tomography. Geoderma 213:471–477. doi:10.1016/j.geoderma.2013.08.034

Sammartino, S., A.-S. Lissy, C. Bogner, R.V.D. Bogaert, Y. Capowiez, S. Ruy, and S. Cornu. 2015. Identifying the functional macropore network related to preferential flow in structured soils. Vadose Zone J. 14(10). doi:10.2136/vzj2015.05.0070

van den Bos, R., L. Hoffmann, J. Juilleret, P. Matgen, and L. Pfister. 2006. Regional runoff prediction through aggregation of first-order hydrological process knowledge: A case study. Hydrol. Sci. J. 51:1021–1038. doi:10.1623/hysj.51.6.1021

van der Walt, S., J.L. Schönberger, J. Nunez-Iglesias, F. Boulogne, J.D. Warner, N. Yager, et al. 2014. Scikit-image: Image processing in Python. PeerJ 2:e453. doi:10.7717/peerj.453

van Schaik, L. 2009. Spatial variability of infiltration patterns related

to site characteristics in a semi-arid watershed. Catena 78:36–47. doi:10.1016/j.catena.2009.02.017

van Schaik, L., R.F.A. Hendriks, and J. van Damm. 2010. Parameterization of macropore flow using dye-tracer infiltration patterns in the SWAP model. Vadose Zone J. 9:95–106. doi:10.2136/vzj2009.0031

van Schaik, L., J. Palm, J. Klaus, E. Zehe, and B. Schröder. 2013. Linking spatial earthworm distribution to macropore numbers and hydrological effectiveness. Ecohydrology 7:401–408. doi:10.1002/eco.1358

Schindler, U., 1980. Ein Schnellverfahren zur Messung der Wasserleitfähigkeit im teilgesättigten Boden an Stechzylinderproben. Arch. Acker-Pflanzenbau Bodenkd. 24:1–7.

Schneider, A.-K., L. van Schaik, A. Zangerlé, T.L. Hohenbrink, and B. Schröder. 2017. Linking earthworm activity and hydrologically effective macropores in space and time, In: Abstracts, 19th General Assembly, European Geosciences Union, Vienna, Austria. 23–28 Apr. 2017. Eur. Geosci. Union, Munich, Germany. p. 9770.

Shipitalo, M.J., and K.R. Butt. 1999. Occupancy and gegeometric properties of *Lumbricus terrestris* L. burrows affecting infiltration. Pedobiologia 43:782–794. doi:10.1078/0031-4056-00232

Šimůnek, J., N.J. Jarvis, M.Th. van Genuchten, and A. Gärdenäs. 2003. Review and comparison of models for describing non-equilibrium and preferential flow and transport in the vadose zone. J. Hydrol. 272:14–35. doi:10.1016/S0022-1694(02)00252-4

Sněhota, M., M. Císlerová, M.H.G. Amin, and L.D. Hall. 2010. Tracing the entrapped air in heterogeneous soil by means of magnetic resonance imaging. Vadose Zone J. 9:373–384. doi:10.2136/vzj2009.0103

Weiler, M. 2005. An infiltration model based on flow variability in macropores: Development, sensitivity analysis and applications. J. Hydrol. 310:294–315. doi:10.1016/j.jhydrol.2005.01.010

Weiler, M., and H. Flühler. 2004. Inferring flow types from dye patterns in macroporous soils. Geoderma 120:137–153. doi:10.1016/j.geoderma.2003.08.014

Weiler, M., and F. Naef. 2003. An experimental tracer study of the role of macropores in infiltration in grassland soils. Hydrol. Processes 17:477–493. doi:10.1002/hyp.1136

Weiler, M.H. 2001. Mechanisms controlling macropore flow during infiltration. Ph.D. diss., Eidgenössische Tech. Hochsch., Zurich. doi:10.3929/ethz-a-004180115

Zangerlé, A., C. Hissler, M. Blouin, and P. Lavelle. 2014. Near infrared spectroscopy (NIRS) to estimate earthworm cast age. Soil Biol. Biochem. 70:47–53. doi:10.1016/j.soilbio.2013.11.023

Zehe, E., U. Ehret, L. Pfister, T. Blume, B. Schröder, M. Westhoff, et al. 2014. HESS opinions: From response units to functional units: A thermodynamic reinterpretation of the HRU concept to link spatial organization and functioning of intermediate scale catchments. Hydrol. Earth Syst. Sci. 18:4635–4655. doi:10.5194/hess-18-4635-2014

Zehe, E., and H. Flühler. 2001. Slope scale variation of flow patterns in soil profiles. J. Hydrol. 247:116–132. doi:10.1016/S0022-1694(01)00371-7

Zehe, E., and C. Jackisch. 2016. A Lagrangian model for soil water dynamics during rainfall-driven conditions. Hydrol. Earth Syst. Sci. 20:3511–3526. doi:10.5194/hess-20-3511-2016

Zehe, E., T. Maurer, J. Ihringer, and E. Plate. 2001. Modeling water flow and mass transport in a loess catchment. Phys. Chem. Earth, Part B: Hydrol. Oceans Atmos 26:487–507. doi:10.1016/S1464-1909(01)00041-7